ITM Web of Conferences 6, 01001 (2016)
DOI: 10.1051/itmconf/20160601001
© Owned by the authors, published by EDP Sciences, 2016

Algorithm for motion control of an exoskeleton during verticalization

Sergey Jatsun[1, a], Sergei Savin[1], Boris Lushnikov[1] and Andrey Yatsun[1]

[1]Southwest State University, Department of mechanics, mechatronics and robotics, 305040 Kursk, Russia

Abstract. This paper considers lower limb exoskeleton that performs sit-to-stand motion. The work is focused on the control system design. An application of a null space projection methods for solving inverse kinematics problem is discussed. An adaptive multi-input multi-output regulator for the system is presented with the motivation for that choice. Results of the simulation for different versions of the regulator are shown.

1 Introduction

The design of exoskeletons is a relevant complex scientific and engineering task. The importance of exoskeleton design can be explained by the wide spectrum of their application in medicine, the military and industry, rehabilitation and improving the life of elderly and disabled people. The complexity of designing effective exoskeletons lies in high demands on the quality of the control system's operation.

At the moment there is a large amount of scientific literature devoted to exoskeleton control, reception and processing of commands from the operator of the exoskeleton (see, for example, [1-2]). Publication [3] discusses issues related to the design of the control system of the exoskeleton as a whole and notes that the low robustness of the resulting control system requires the use of a high-precision control system dynamic model of the mechanism. Many publications focus on application of assistive and medical exoskeletons (see [4-7]).

There is a series of work describing exoskeleton control during verticalization (see [8-12]). Article [8] proposed an analytical method of solving the inverse kinematics problem and the control system's structure based on a modified version of a proportional-integral regulator. The stated approach is developed in [9] where it is supplemented by an adaptive module that allows us to change the time allotted to verticalization depending on the load on the exoskeleton. The regulator's region of parameters allowing for verticalization of the exoskeleton without tipping was determined in [10] by numerical experiments. A two-stage control strategy for the process of ascent from a chair is developed in [11].

One of the disadvantages of the proposed approaches to exoskeleton control is that the input parameters of the control system are the coordinates of the center of mass and the body's angle of inclination and control system does not cater for a soft transition to another set of control actions. To solve this problem we propose in this work a control strategy that uses the null space projection method (see [13]) of solving the inverse kinematics problem.

2 Description of the lower-limb exoskeleton

We consider a remote controlled lower-limb exoskeleton which is a multi-link system mounted on the operator by means of belts. Each leg of the exoskeleton is a three-link mechanism with successive hinged joints. The exoskeleton's links are driven by electric drives installed in the joints. Fig.1 shows a photograph of an experimental prototype of the exoskeleton.

Figure 1. Photograph of a lower-limb exoskeleton.

The dimensions of the links and the location of the hinges are designed in such a way that the links move

[a]Corresponding author: teormeh@inbox.ru

This is an Open Access article distributed under the terms of the Creative Commons Attribution License 4.0, which permits unrestricted use distribution, and reproduction in any medium, provided the original work is properly cited.

together with the person's body parts to which they are connected.

3 Mathematical model of the mechanism

In this work we look at the exoskeleton's motion during the process of verticalization. We assume that the links and the legs perform planar motion. This allows us to model the exoskeleton as a four-link mechanism with successive hinged joints. The analytical diagram for the mechanism is shown in Fig. 2.

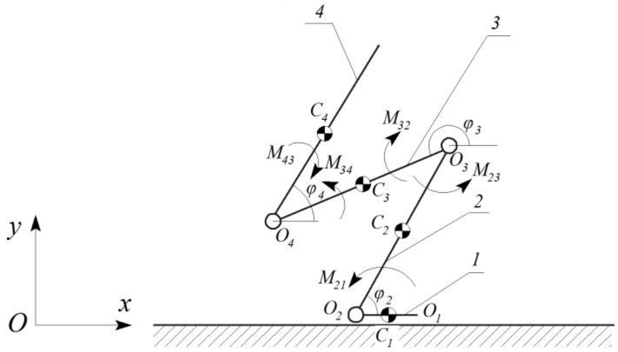

Figure 2. Analytical diagram of the exoskeleton; 1-4 – first – fourth links.

On Fig. 2 we have C_i – the centers of mass of the links and points O_i – locations of the hinged joints. Angles φ_i determine the orientation of the links relative to the horizontal plane, $M_{i,i-1}$ – torques applied to the links by the mechanism. The links have masses m_i, lengths l_i and moments of inertia relative their centers of mass equal to I_i. We make the assumption that the first link is fixed during motion.

We introduce a vector of joint coordinates: $\vec{q} = \begin{bmatrix} \varphi_2 & \varphi_3 & \varphi_4 \end{bmatrix}^{\mathrm{T}}$. Kinematic and dynamic equations of the given mechanism can be written using the introduced denotations. Here we confine ourselves to the vector form of the equations of motion (the scalar form can be found in [11]):

$$\mathbf{A}(\vec{q})\ddot{\vec{q}} = \vec{b}(\vec{q},\dot{\vec{q}}) + \mathbf{B}\vec{M} \tag{1}$$

where $\mathbf{A}(\vec{q})$ – joint space inertial matrix, $\dot{\vec{q}}$ – vector of joint velocities, $\ddot{\vec{q}}$ – vector of joint accelerations, $\vec{b}(\vec{q},\dot{\vec{q}})$ – vector of joint gravitational forces and inertial forces. $\vec{M} = \begin{bmatrix} M_{21} & M_{32} & M_{43} \end{bmatrix}^{\mathrm{T}}$ – vector of the torques of the electric drives, $\mathbf{B}$ – quadratic matrix.

Matrix $\mathbf{A}(\vec{q})$ is found by the formula: $\mathbf{A}(\vec{q}) = \partial^2 T / \partial\dot{\vec{q}}\partial\dot{\vec{q}}$; matrices $\mathbf{A}$ and $\mathbf{B}$ are as follows:

$$\mathbf{A} = \begin{bmatrix} a_{11} & a_{12} & a_{13} \\ a_{12} & a_{22} & a_{23} \\ a_{13} & a_{23} & a_{33} \end{bmatrix}, \mathbf{B} = \begin{bmatrix} 1 & -1 & 0 \\ 0 & 1 & -1 \\ 0 & 0 & 1 \end{bmatrix},$$

where $a_{11} = l_2^2\left(m_2/4 + m_3 + m_4\right) + I_2$

$a_{12} = l_2 l_3 \cos\left(\phi_2 - \phi_3\right)\left(m_3/2 + m_4\right)$,

$a_{13} = 0.5\cos\left(\phi_2 - \phi_4\right) l_2 l_4 m_4$, $\quad a_{22} = l_2^2\left(m_3/4 + m_4\right) + I_3$,

$a_{23} = 0.5\cos\left(\phi_3 - \phi_4\right) l_3 l_4 m_4$, $a_{33} = l_4^2 m_4/4 + I_4$.

4 Control system

Here the control problem is verticalization of the exoskeleton i.e. executing vertical displacement of its centre of mass (CM). We consider the case when the desired displacement of the CM in the vertical direction is described by the polynomials:

$$x_C^*(t) = \sum_{p=0}^{n}\left(t^p \cdot c_{1,p}\right), \tag{2}$$

$$y_C^*(t) = \sum_{p=0}^{n}\left(t^p \cdot c_{2,p}\right). \tag{3}$$

The method of acquiring such polynomials which provide motion with zero velocity at the initial and final times, while observing constraints on horizontal displacement of the CM. Here we will consider the case when the CM moves vertically up.

We can find the desired values of generalized coordinates by solving the inverse kinematics problem given the desired trajectory of the center of mass. We need to define another function of generalized coordinates (in papers [13-16] such function is called "tasks" and we will use this term from here on) to obtain a unique solution of the inverse kinematics problem since we have 3 generalized coordinates and only two equations for x_C^* and y_C^*. An example is the task of controlling the horizontal position of the head of a person wearing an exoskeleton:

$$x_{O5}^*(t) = \sum_{i=2}^{4} l_i \cos(\varphi_i) = h = const\ . \tag{4}$$

We need task differential kinematics equations to use the null space projection method:

$$\dot{\vec{r}}_N^* = \begin{bmatrix} \dot{x}_N^* \\ \dot{y}_N^* \end{bmatrix} = \mathbf{J}_1 \begin{bmatrix} \dot{\varphi}_2 \\ \dot{\varphi}_3 \\ \dot{\varphi}_4 \end{bmatrix},\ \dot{x}_{O5}^* = \mathbf{J}_2 \begin{bmatrix} \dot{\varphi}_2 \\ \dot{\varphi}_3 \\ \dot{\varphi}_4 \end{bmatrix}, \tag{5}$$

where $\mathbf{J}_1$, $\mathbf{J}_2$ are task Jacobians given by:

$$\mathbf{J}_1 = \begin{bmatrix} -K_2\sin(\varphi_2) & -K_3\sin(\varphi_3) & -K_4\sin(\varphi_4) \\ K_2\cos(\varphi_2) & K_3\cos(\varphi_3) & K_4\cos(\varphi_4) \end{bmatrix}, \tag{6}$$

$$\mathbf{J}_2 = \left[-l_2\sin(\varphi_2) \quad -l_3\sin(\varphi_3) \quad -l_4\sin(\varphi_4)\right]. \tag{7}$$

The following equations describe the operation of the null space projection method as applied to this problem:

$$\dot{\vec{q}}^* = \vec{s} + \left(\mathbf{J}_2\mathbf{P}\right)^+\left(\dot{x}_{O5}^* - \mathbf{J}_2\vec{s}\right), \tag{8}$$

$$\vec{s} = \mathbf{J}_1^+\dot{\vec{r}}_N^*,\ \ \mathbf{P} = \mathbf{I} - \mathbf{J}_1^+\mathbf{J}_1,$$

where $\vec{s}$ are the generalized velocities needed to perform the first task alone, $\mathbf{P}$ is an orthogonal projector, $\mathbf{I}$ is an identity matrix; the sign $^+$ denotes the Moore-Penrose pseudo inverse of a matrix. The value for $\vec{q}^*$ is obtained by integrating the previously obtained $\dot{\vec{q}}^*$.

This method also allows setting priorities to the tasks, the associated methodology can be found in paper [13].

This work considers error based control. The control error is evaluated as the difference between the desired and current values of joint coordinates:

$$\vec{e} = \vec{q}^* - \vec{q} \,. \tag{9}$$

We pose the problem of synthesizing a regulator providing exponential tendency of error to zero. This can be achieved if the error satisfies the following vector differential equation:

$$\frac{d^2}{dt^2}\vec{e} + \mathbf{K}_d \frac{d}{dt}\vec{e} + \mathbf{K}_p\vec{e} = 0 \,, \tag{10}$$

where $\mathbf{K}_d, \mathbf{K}_p$ are diagonal matrices with positive elements.

Using (9) and expressing $\ddot{\vec{q}}$ from (1) and substituting it here we get:

$$\ddot{\vec{q}}^* + \mathbf{K}_d \frac{d}{dt}\vec{e} + \mathbf{K}_p\vec{e} = \mathbf{A}^{-1}b + \mathbf{A}^{-1}\mathbf{B}\vec{M} \,. \tag{11}$$

We express $\vec{M}$ from the obtained formula:

$$\vec{M} = \mathbf{B}^{-1}\mathbf{A}\left(\ddot{\vec{q}}^* + \mathbf{K}_d \frac{d}{dt}\vec{e} + \mathbf{K}_p\vec{e}\right) - \mathbf{B}^{-1}b \,. \tag{12}$$

The resulting regulator causes error to tend to zero. The following simplified formula can be used to simplify the realization of the regulator:

$$\vec{M} = \mathbf{B}^{-1}\mathbf{A}\left(\mathbf{K}_d \frac{d}{dt}\vec{e} + \mathbf{K}_p\vec{e}\right). \tag{13}$$

Taking into account the written expressions the exoskeleton's control system acquires a structure shown in Fig. 3.

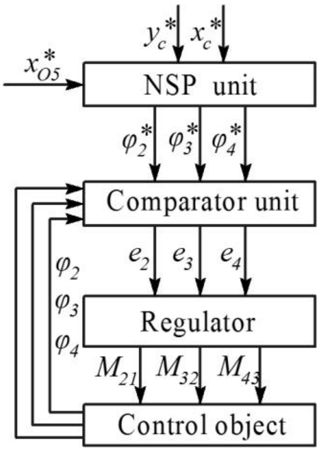

Figure 3. Structural diagram of the control system.

Fig. 3 shows five blocks of the control system. Block NSP Unit solves the inverse kinematics problem using equations (8); The Comparator block computes the control error's current values; the Regulator block generates control actions according to equation (13). The action of the block, Controlled Object is described by equation (1).

5 Results of numerical modeling conclusion

We use the following values of the mechanism's parameters during modeling: $m_2 = 9.6$ kg, $m_3 = 16.8$ kg, $m_4 = 53.6$ kg, $l_2 = 0.51$ m, $l_3 = 0.51$ m, $l_4 = 0.68$ m. The stated values were obtained using the parameter selection method, which allows consideration of weight and size parameters of both the exoskeleton and the operator. This method is described in [17].

We consider the case when the mechanism performs the following tasks:

$$x_{O5}^*(t) = x_{O5}^*(0), \;\; x_C^*(t) = x_C^*(0), \tag{14}$$

$$y_C^*(t) = 0.363 + 0.0161 \cdot t^2 - 0.0011 \cdot t^3 \,. \tag{15}$$

Formulas (14) imply that the horizontal position of the center of mass and O_5 must not change during motion. Fig. 4 shows time graphs for this case.

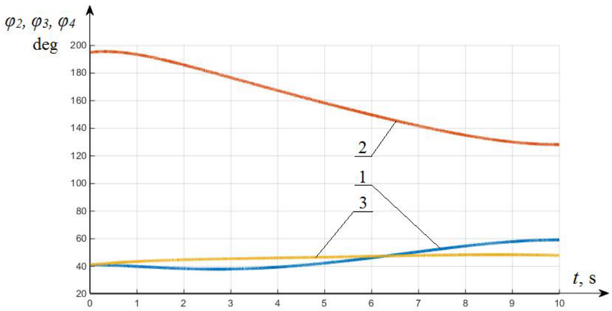

Figure 4. Time graphs of generalized coordinates: 1 – φ_2 ; 2 – φ_3 ; 3 – φ_4 .

Graphs of the desired and obtained values of coordinates visually coincide. In order to demonstrate the operation of the method we use fig. 5 to show the sequence of the positions taken by the mechanism. It can be observed that the centre of mass and point O_5 move vertically upwards without shifting in the horizontal direction, which satisfies the tasks given by formula (14).

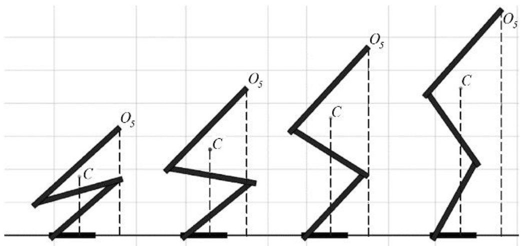

Figure 5. Sequence of positions taken by the mechanism during verticalization.

Fig. 6 presents time graphs of torques generated by the drives of the mechanism during verticalization.

After analyzing the graphs shown above it can be noted that with the exception of rapid changes in the values of moments at the beginning of motion the obtained graphs have the form of smooth continuously varying functions. We note that in practice the problem of abrupt changes in torque values at the beginning of the motion mechanism is mitigated by the fact that exoskeleton rests on chair at the beginning of motion, so that in the event that the control system is unable to execute a sufficiently rapid increase of the torques it will only result in the time lag of visible verticalization. The introduction of elastic elements in the exoskeleton's structure allows us to make the change of torques at the beginning of motion much smoother.

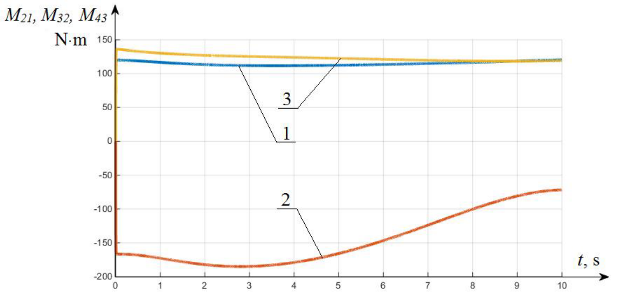

Figure 6. Time graphs of torques graphs of torques generated by the drives during verticalization: 1 – $M_{21}(t)$; 2 – $M_{32}(t)$; 3 – $M_{43}(t)$.

Let us assess the difference between controls given by expressions (12) and (13). To do that an expression for $\ddot{\vec{q}}^*$ is needed. We derive it in the following way:

$$\ddot{\vec{q}}^* = \left(\frac{\partial \vec{r}_t}{\partial \vec{q}}\right)^{-1}\left(\ddot{\vec{r}}_t - \frac{\partial \dot{\vec{r}}_t}{\partial \vec{q}}\dot{\vec{q}}\right), \quad (16)$$

where $\vec{r}_t = [x_C \quad y_C \quad x_{O5}]^{\mathrm{T}}$.

The time dependencies for generalised coordinates obtained using control given by (12) will be denoted as $\vec{q}^{<1>}$, and for the case when controls are given by (13) those dependencies will be denoted as $\vec{q}^{<2>}$. Difference between the them will be denotes as $\vec{\varepsilon}$:

$$\vec{\varepsilon} = \vec{q}^{<2>} - \vec{q}^{<1>}. \quad (17)$$

The graphs of ε_1, ε_2 and ε_3 are plotted in Fig. 7.

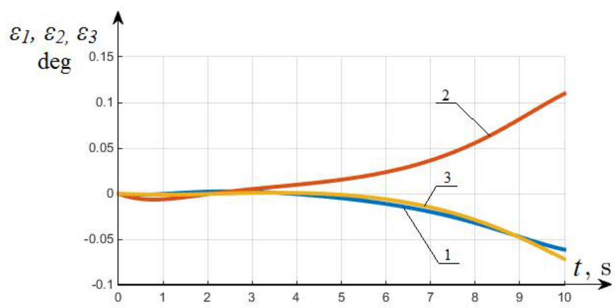

Figure 7. Time graphs of differences betwean generalised coordinates obtained using controls given by expressions (12) and (13): 1 – $\varepsilon_1(t)$, 2 – $\varepsilon_2(t)$, 3 – $\varepsilon_3(t)$.

From the graphs in the Fig. 7, we can see that the difference between the angles is less than 0.15 degree in absolute value. The difference between control errors for two controls is bounded by 0.1 degree in absolute value. That suggests that for some practical applications the difference between performances of two controls is not significant, while the scheme given by the expression (13) is simpler to implement and requires less knowledge of the control object.

6 Conclusion

An algorithm of the automatic control system's operation using the null space projection method for solving the inverse kinematics problem with multiple tasks was demonstrated in this work. The synthesis of a multichannel regulator that performs error based control was described. The efficiency of the proposed system was demonstrated by numerical experiments and an analysis of the obtained graphs was done. The developed approach to exoskeleton control during verticalization was used during in the design of the automatic control system for the prototype – ExoLite, undergoing tests at the laboratory of mechatronics and robotics at Southwest State University.

Acknowledgments

Work is supported by RSF, Project № 14-39-00008

References

1. J. Rosen, M. Brand, M.B. Fuchs and M. Arcan. IEEE Transactions on Systems, Man and Cybernetics, Part A: Systems and Humans, **31**, 210 (2001)
2. K. Kiguchi, T. Tanaka and T. Fukuda. IEEE Transactions on Fuzzy Systems, **12**, 481 (2004)
3. H. Kazerooni, J.L. Racine, L. Huang and R. Steger. Proceedings of the 2005 IEEE international conference on Robotics and automation ICRA 2005, pp. 4353-4360 (2005).
4. Y. Mao, X. Jin, G.G. Dutta, J.P. Scholz and S.K. Agrawal. IEEE Transactions on Neural Systems and Rehabilitation Engineering, **23**, 84 (2015)
5. K.Z. Takahashi, M.D. Lewek and G.S. Sawicki. Journal of neuroengineering and rehabilitation, **12**, 23 (2015)
6. E.A. Rogers. Assistive Exoskeleton for Injury Prevention During Downhill Walking. Bachelor's thesis (Harvard College, 2015)
7. X. Jin, X. Cui and S.K. Agrawal. *2015 IEEE International Conference on Robotics and Automation (ICRA),* pp. 5578-5583 (2015)
8. S. Jatsun, S. Savin, A. Yatsun, and A. Malchikov. *Advances in Robot Design and Intelligent Control. Springer International Publishing*. pp. 165-172 (2016)
9. S. Jatsun, S. Savin, A. Yatsun and R. Turlapov. *2015 10th International Symposium on Mechatronics and its Applications (ISMA)*, pp. 1-6 (2015).
10. S.F. Jatsun, S.I. Savin, A.S. Yatsun and R.N. Turlapov. *26th DAAAM International Symposium on Intelligent Manufacturing and Automation*. (2015).
11. S. Jatsun, S. Savin, A. Yatsun, I. *Performing Standing up Motion from a Chair Proceedings of 4th International Conference on Robot Intelligence Technology and Applications (RiTA)* (2015)
12. S.F. Jatsun, L.Yu. Vorochaeva, A.S. Yatsun and S.I. Savin. *Proceedings of the International Conference on CLAWAR*, pp. 175-182 (2015)

13. F. Flacco, A. De Luca and O. Khatib. IEEE Transactions on Robotics, **31**, 637 (2015)
14. F. Flacco, A. De Luca, and O. Khatib. *2012 IEEE/RSJ International Conference on Intelligent Robots and Systems (IROS)*, pp. 3970-3977 (2012)
15. J. Nakanishi, R. Cory, M. Mistry, J. Peters and S. Schaal. *2005 IEEE/RSJ International Conf. Intelligent Robots and Systems, (IROS 2005)* (2005)
16. L. Sentis and O. Khatib. *IEEE International Conference on Humanoid Robots* (2004)
17. S. Jatsun, S. Savin, A. Yatsun. *Proceedings of 21st CISM-IFToMM Symposium on Robot Design 2016* (in publishing)